01 Nov 2011

Comparison of Microwave and Conventionally Sintered Yttria-Doped Zirconia Ceramics

Colin J. Reidy

Thomas J. Fleming

Stuart Hampshire

Mark R. Towler
Missouri University of Science and Technology, mtowler@mst.edu

Recommended Citation

C. J. Reidy et al., "Comparison of Microwave and Conventionally Sintered Yttria-Doped Zirconia Ceramics," *International Journal of Applied Ceramic Technology*, vol. 8, no. 6, pp. 1475 - 1485, Wiley, Nov 2011.
The definitive version is available at https://doi.org/10.1111/j.1744-7402.2011.02608.x

Int. J. Appl. Ceram. Technol., 8 [6] 1475–1485 (2011)
DOI:10.1111/j.1744-7402.2011.02608.x

International Journal of
Applied Ceramic TECHNOLOGY
Ceramic Product Development and Commercialization

Comparison of Microwave and Conventionally Sintered Yttria-Doped Zirconia Ceramics

Colin J. Reidy, Thomas J. Fleming, and Stuart Hampshire*

Materials and Surface Science Institute, University of Limerick, Limerick, Ireland

Mark R. Towler

Inamori School of Engineering, Alfred University, Alfred, New York 14802

This paper reports on improvement of the physical and mechanical properties of Y_2O_3–ZrO_2 ceramics through compositional optimization, the use of nanograined powders and utilization of microwave sintering. ZrO_2 with 2–5 mol% Y_2O_3, prepared from nanopowders, was sintered in both conventional and microwave furnaces under exactly the same heating schedule. It was found that microwave sintering improves physical and mechanical properties of Y_2O_3–ZrO_2 ceramics compared with conventional sintering. Compositions containing 2 mol% Y_2O_3 exhibit the greatest improvement due to retention of tetragonal ZrO_2, with a 5% increase in relative density compared with conventional sintering. Grain size analysis indicated that there was significant grain growth in microwave sintered (MWS) samples (353 nm) compared with their conventionally sintered (CS) counterparts (200 nm) which is thought to be related to enhanced diffusional effects during microwave sintering. Associated with this was a 22% increase in Young's modulus to 220 GPa, a 77% increase in Vicker's Hardness up to 11.5 GPa and a 165% increase in biaxial flexural strength up to 800 MPa. Owing to the differences in physical and mechanical properties along with the altered phase assemblages produced, it is apparent that microwave heating provides an additional driving force during sintering which enhances diffusion processes.

Introduction

Zirconia (ZrO_2) is a refractory material with a range of properties such as high fracture toughness, high hardness and wear resistance, chemical inertness,

This work was funded by Enterprise Ireland—Technology Development Grant EI/TD/2006/0328.

*stuart.hampshire@ul.ie

low thermal conductivity, ionic conductivity which allows its use in a range of applications including precision ball valve balls, high-density ball-mill grinding media, rollers and guides for metal tube forming, thread guides, pump seals, oxygen sensors, and solid oxide fuel cell membranes. These properties and applications are only realized through controlled processing of partially stabilized zirconias (PSZ) with alkaline earth or rare earth oxide additions, such as yttria (Y_2O_3), to produce tailored microstructures that make positive use of the tetragonal ZrO_2 (*t*-ZrO_2) to monoclinic ZrO_2 (*m*-ZrO_2) phase transformation to enhance properties through transformation toughening.[1–3] Typical microstructures for this family of ceramics consist of tetragonal phase precipitates in a cubic ZrO_2 (*c*-ZrO_2) ceramic matrix (PSZ) or simply single-phase tetragonal ZrO_2 polycrystals (TZP). The good mechanical properties, in combination with biocompatibility, have made Y_2O_3-doped ZrO_2-based ceramics suitable for dental implant applications. Three and 8 mol% Y_2O_3 are the most widely studied dopant concentrations as these compositions are sufficient to form single-phase *t*-ZrO_2 and fully stabilized *c*-ZrO_2 respectively.[4,5] *t*-ZrO_2 possesses higher mechanical properties than *c*-ZrO_2, which is attributed to transformation toughening associated with the tetragonal–monoclinic phase transformation.[1–3,6]

Sintering of zirconia ceramics using microwaves of various frequencies (2.45–60 GHz) has previously been studied.[7–13] In conventional thermal processing, energy is transferred to the material through conduction and radiation of heat from the surface. In contrast, microwave energy is delivered directly to the material through molecular interaction with the electromagnetic field.[14] This interaction leads to various beneficial effects, including rapid volumetric heating, shorter sintering times, lower sintering temperatures, selective heating, and an additional driving force for diffusion mechanisms, the so-called "microwave effect."[13,15,16] Wang *et al.*[13] used a microwave/conventional hybrid heating regime for various ceramics including zirconia where it was ensured that each sample within a series had an identical thermal history in terms of its temperature/time profile. The results showed that grain growth was enhanced during microwave/conventional hybrid heating compared with pure conventional heating suggesting that microwave sintering resulted in an acceleration of the diffusional processes involved.

The aim of the present work was to make a direct comparison between microwave sintering and conventional sintering for ZrO_2 green compacts doped with from 2 to 5 mol% Y_2O_3 created from nanoscale Y_2O_3 and ZrO_2 powders. The conventional sintering followed exactly the same heating schedule as the microwave-sintering regime in order to confirm if a "microwave effect" exists for these materials. If successful, microwave sintering may be a useful processing route for dental and biomedical zirconia ceramics.

Experimental Procedure

Powder and Compact Preparation

Commercial coprecipitated 3 and 8 mol% Y_2O_3–ZrO_2 (TZ-3Y and TZ-8Y, Tosoh, Tokyo, Japan) powders were mixed with Y_2O_3-free monoclinic powder (TZ-0, Tosoh) in order to obtain mixtures with an overall Y_2O_3 content of 2, 3, 4, and 5 mol%. The addition of Y_2O_3-free ZrO_2 to coprecipitated ZrO_2 powders has been shown to increase the mechanical properties of sintered ZrO_2 ceramics over coprecipitated powders with similar Y_2O_3 content.[6] Powders were attrition milled, shell frozen, and retrieved using a freeze dryer to obtain a homogenous mixture. The resultant powder was passed through a 90 μm sieve in order to break up soft agglomerates. Particle size was analyzed by laser diffraction (Malvern Mastersizer 2000, Malvern, U.K.) and transmission electron microscopy (TEM, JEM-2011, JEOL, Tokyo, Japan).

Powders were then uniaxially pressed to 35 MPa in a ∅ 20 mm stainless-steel die and subsequently isostatically pressed at 150 MPa to produce disk-shaped green bodies (∅ 19 mm, h 3 mm).

Conventional and Microwave Sintering

Samples were microwave sintered (MWS) using a single-mode microwave furnace with a cavity of 33 cm × 22 cm × 31 cm lined with an alumino-silicate fiberboard insulating material (Fiberfrax Duraboard™, Unifrax LLC, Niagara Falls, NY). Power is provided by a 1.45 kW magnetron (I.B.F. Electronic, Ober-Ramstadt, Germany), which is regulated by a programmable process controller (Eurotherm 3214, Eurotherm, Worthing, U.K.). Temperature is measured using an optical pyrometer (Land Instruments International, Dronfield, U.K.) focused directly onto the samples. The pyrometer is directly connected to the controller and does not influence or interfere with the microwave

field distribution within the cavity. Traditional metal thermocouples can interfere with the microwave field within the cavity preventing accurate measurements from being made. The pyrometer was calibrated at several temperature points using a type B PtRh thermocouple placed in contact with the samples when the magnetron was deactivated. The small thickness of the samples ensures that axial temperature gradients are small.

The homogeneity of the field within the cavity was tested by lining the floor of the furnace with sample vials containing 2 mL of distilled water, running the magnetron for a short time and measuring the temperature of the individual vials using an electronic thermometer probe (Accumet®, Fisher Scientific Ireland, Dublin, Ireland).

A hybrid heating method utilized a nested crucible assembly with a surrounding silicon carbide (SiC) layer into which the green zirconia bodies to be fired were inserted ($n = 9$ per firing). This method minimizes thermal gradients within the individual samples and homogenizes the temperature within the crucible itself through mutual heating, while providing the ability to conventionally heat them to a critical temperature beyond which they heat solely due to microwave radiation absorption.[17] Samples were exposed to $\sim$700 W of microwave energy, which allowed them to follow the typical microwave heating profile shown in Fig. 1. From $\sim$1200°C onwards, the energy absorption is almost completely balanced by thermal losses from the system and the heating rate decreases markedly.

A maximum sintering temperature of $\sim$1300°C was utilized. The samples were then held for an hour at the process temperature before being allowed to furnace cool. The temperature profile was recorded and subsequently used to program a conventional resistive element sintering furnace (CS) in which comparative firings were performed using the same heating profile.

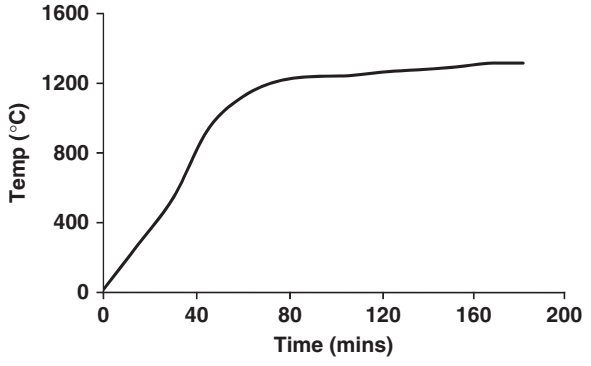

Fig. 1. Typical microwave furnace heating profile.

X-ray Diffraction

In order to examine the phase assemblages of the densified bodies, X-ray diffraction was performed (Philips X'Pert MPD Pro diffractometer, Philips, Eindhoven, The Netherlands). Scans ranged from $5° < 2\theta < 80°$ with a step size of 0.2° and a time per step of 20 s. The volume fraction of m-ZrO_2 was calculated from the relative intensities of the principle m-ZrO_2 and t/c-ZrO_2 peaks in the range 28–32° 2θ.[18]

Physical and Mechanical Properties

Densities of the sintered bodies were determined by an Archimedes method using a Sartorius YDK-01 (Sartorius, Goettingen, Germany) balance accessory kit.

The theoretical density (TD) of zirconia was calculated using the Aleksandrov method[19,20] which takes into account the Y_2O_3 content and therefore allows for the variation in the absolute value of TD with composition.

The elastic modulus was determined using an ultrasonic pulse echo test method based on ASTM E494-10.[21,22] The longitudinal (V_l) and transverse (V_t) ultrasonic wave velocities were determined on each sample with an accuracy better than 0.1% using two 10 MHz piezoelectric transducers (Ultran Laboratories, Boalsburg, PA). The Young's (E) and shear (G) moduli and Poisson's ratio (υ) were calculated from the following equations:

$$E = \rho(3\,V_l^2 - 4\,V_t^2)/[(\,V_l^2/4\,V_t^2) - 1] \quad (1)$$

$$G = \rho\,V_t^2 \quad (2)$$

$$\upsilon = (E/2G) - 1 \quad (3)$$

Samples were then polished to a mirrored finish in steps of 40, 9, 6, and 3 μm with diamond slurry on polishing cloth. Vickers microhardness was determined using a diamond indentor technique (Leco M-400-G1, Leco, St. Joseph, MI) with a load of 1 kg applied for 15 s.

Biaxial flexural strength (BFS) was determined by performing 4 point bending tests adapted from ISO 6872[23] using a Lloyd loadframe LR50 K (Lloyd Instruments, West Sussex, U.K.) with a crosshead speed of 0.1 mm/min and a 5 KN load cell.

Electron Microscopy

TEM imaging was performed (JEOL JEM 2011) using a LaB_6 filament operated at 200 kV in order to confirm the particle size analysis data and to examine crystallite morphology and agglomeration. Using a pipette, one drop of a dispersion of the sample in isopropanol, was dropped onto a 3 mm circular copper grid with a Holey carbon support film and allowed to dry.

Scanning electron microscopy (SEM) and energy-dispersive X-ray analysis (SU70 FE-SEM, Hitachi High-Technologies Europe, Krefeld, Germany) were carried out on the fracture surfaces generated as a result of BFS testing. Grain size was measured using the linear intercept method on more than 200 grains from images randomly selected on the specimens. The average grain size, G, was determined using the relation:

$$G = \frac{1.5L}{MN} \tag{4}$$

where 1.5 is a geometry-dependent proportionality constant, L is the total test line length, M is the magnification, and N is the total number of intercepts.

Results

Particle Size

Particle size data is presented in Table I. The particle size obtained by laser diffraction ($d_{(50)}$) indicates that the particles possess an equivalent spherical diameter of the order of 160 nm. BET measurements ($S_{(BET)}$) indicate that the mixed powders have specific surface areas in the range 15–23 m^2/g. Assuming that the particles have a spherical shape with a smooth surface and a similar size, the surface area can be related to the average particle size using the following equation:

$$D_{(BET)} = 6000/(\rho S_{(BET)}) \tag{5}$$

where $D_{(BET)}$ is the average particle size (nm) from surface area measurements, ρ is the density (g/cm^3), and $S_{(BET)}$ is the specific surface area (m^2/g).

Table I. Particle Size Data for Y_2O_3-Doped Zirconia

Mol% Y_2O_3	2	3	4	5
$S_{(BET)}$ (m^2/g)	23.4	17.4	15.4	18.8
$D_{(BET)}$ (nm)	42	57	65	53
$d_{(50)}$ (nm)	146	170	163	160

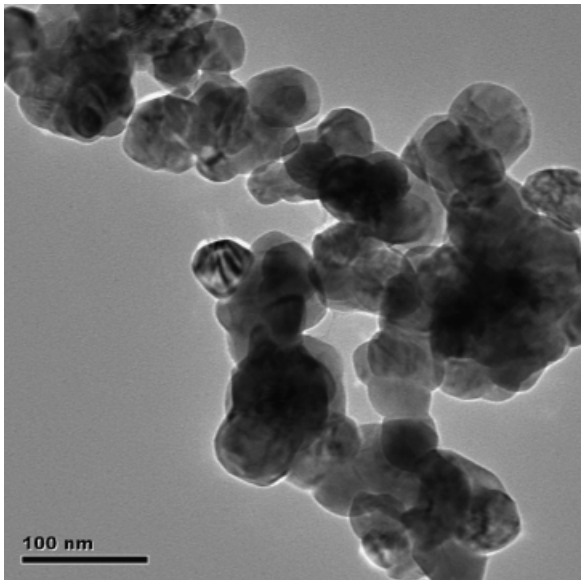

Fig. 2. TEM image of 2 mol% Y_2O_3-doped ZrO_2 powder.

This is an established technique of avoiding agglomeration when analyzing nanopowders.[24–26] This calculation gives particles with an equivalent spherical diameter within the range ~42–65 nm, approximately one-third that of the $d_{(50)}$ value. This may indicate that the ZrO_2 powders are prone to water-induced agglomeration and sonication is insufficient to disrupt all agglomerates. For all measurements there is no direct correlation between Y_2O_3 content and particle size.

A typical TEM image of the ZrO_2 doped with 2 mol% Y_2O_3 is presented in Fig. 2. Individual, rounded, grains $\varnothing$ ~50 nm are agglomerated into larger structures several hundred nanometers across. The size of the spherical morphology of the particles observed by TEM coincides with the results obtained from the BET particle size measurement. Considering the mean particle size obtained from the laser diffraction technique, which involves sonication of a suspension of the powder, it appears that the ZrO_2 powders are prone to agglomeration when exposed to water that cannot be entirely removed through sonication. Similar results for Tosoh 3Y–ZrO_2 has been observed by Hasanuzzaman *et al.*[26]

Physical Properties

Upon initial visual inspection following sintering, it was found that the MWS samples were all approximately the same thickness and diameter, except the

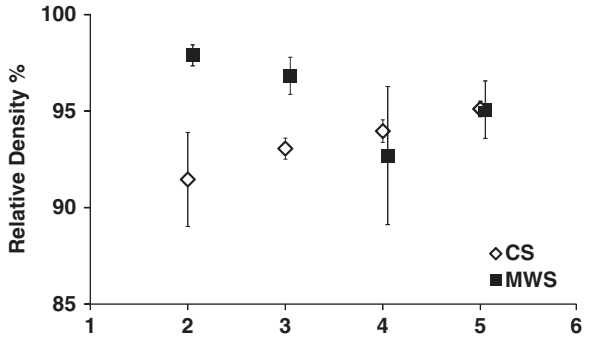

Fig. 3. Effect of Y_2O_3 content on relative density of microwave sintered (MWS) and conventionally sintered (CS) ZrO_2.

ZrO_2 doped with 4 mol% Y_2O_3 which experienced some assymetrical shrinkage and cracking and hence resulted in larger deviations in density and porosity. The reason for the cracking is not readily apparent as the powder characteristics were similar for all compositions.

It can be seen from Fig. 3 that the relative densities of the conventionally sintered (CS) ZrO_2 bodies increase linearly with Y_2O_3 content, from 90% at 2 mol% Y_2O_3 content to 95% at 5 mol% Y_2O_3 content. The relative densities of the MWS ZrO_2 containing 2 and 3 mol% Y_2O_3 are ~95.5–97%, which is greater than their CS counterparts. Considering the assymetrical shrinkage and slight cracking for ZrO_2 samples containing 4 mol% Y_2O_3, there is a linear trend in relative density from ~97% at 2 mol% Y_2O_3 to ~95% at 5 mol% Y_2O_3 and at this level of Y_2O_3, densities are similar to their CS counterparts.

From Fig. 4, it can be seen that the open porosity of the sintered bodies follows an inverse trend to that of relative density in Fig. 3. The open porosity of the CS

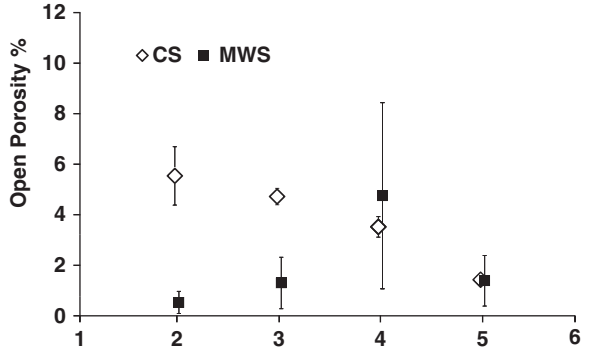

Fig. 4. Effect of Y_2O_3 content on open porosity of microwave sintered (MWS) and conventionally sintered (CS) ZrO_2.

ZrO_2 decreases linearly with Y_2O_3 content, from ~6% (±2%) at 2 mol% Y_2O_3 content to ~1% at 5 mol% Y_2O_3 content. The open porosity of the MWS ZrO_2 increases with Y_2O_3 content, from 1% at 2 mol% Y_2O_3 content to 5% (±4%) at 4 mol% Y_2O_3 content, this wide variation reflecting the defects in these latter samples. There is a subsequent reduction in porosity, down to 2% (±1%) with the addition of 5 mol% Y_2O_3. It must be noted that below 4 mol% Y_2O_3 content the open porosities of the MWS materials are lower than those of their CS counterparts, whereas above 4 mol% Y_2O_3 content there is no statistical difference.

The narrow spread in standard deviations exhibited by the MWS samples (except for the cracked ZrO_2 samples with 4 mol% Y_2O_3) reinforces the results of earlier measurements of microwave field homogeneity within the cavity.

X-ray Diffraction

Figure 5 shows X-ray diffraction patterns of the ZrO_2 ceramics doped with 2–5 mol% Y_2O_3 (a) MWS and (b) CS at 1300°C. The peak at $2\theta = 30^\circ$ associated with *t*-ZrO_2 and *c*-ZrO_2 is observed in all diffractograms regardless of sintering method or Y_2O_3 content. The coalescence of the twin peaks at $2\theta = 35^\circ$ with increasing Y_2O_3 content indicates that *c*-ZrO_2 is being formed at the expense of the tetragonal phase. The primary difference in sintering methods is more noticeable for the ZrO_2 with 2 mol% Y_2O_3 content. The CS samples exhibit peaks at $2\theta = 28^\circ$ and 32° and from the calculations of intensities of the different peaks, this corresponds to ~86% *m*-ZrO_2 with the remainder being *t*-ZrO_2. The MWS samples possess a slight broad peak at $2\theta = 28^\circ$, which indicates from calculations of intensities that they contain ~6% *m*-ZrO_2 and ~94% *t*-ZrO_2. It is clear that MWS is more effective at stabilizing the *t*-ZrO_2 phase at this "lower" sintering temperature of 1300°C and also that 2 mol% Y_2O_3 is insufficient to stabilize the *t*-ZrO_2 phase at a conventional sintering temperature of 1300°C. This suggests that microwave energy provides an additional driving force during sintering, a so-called "microwave effect" which has been reported previously.[13,16]

Mechanical Properties

Figure 6 shows the effect of Y_2O_3 content on Young's modulus of MWS and CS ZrO_2 materials.

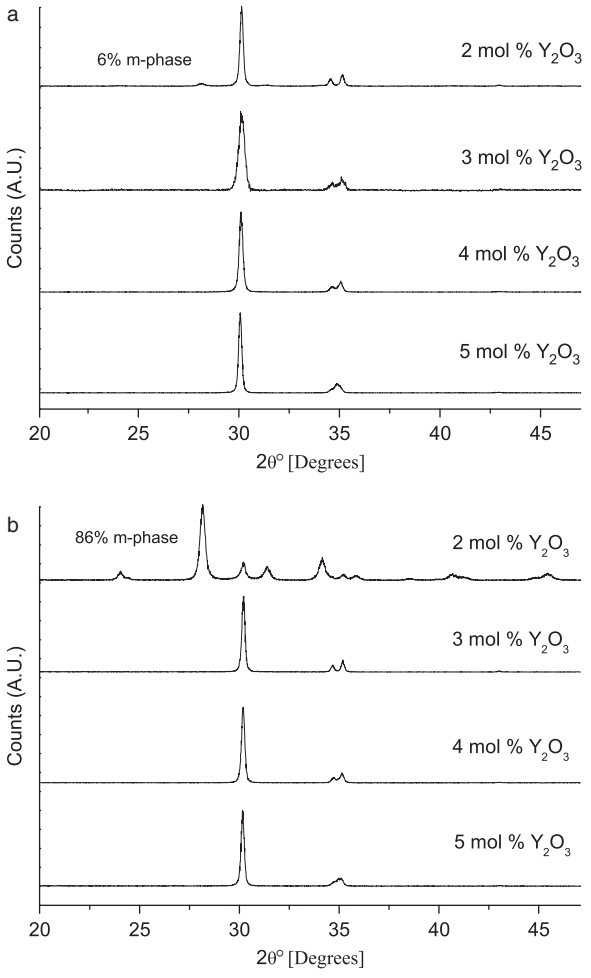

Fig. 5. X-ray diffraction patterns of Y_2O_3-doped ZrO_2 ceramics (a) microwave sintered (b) conventionally sintered at 1300°C.

The trends for both sintering regimes are similar to those for the relative densities. The Young's moduli of the CS ZrO_2 materials increase linearly with increasing Y_2O_3 content, from 180 (±15) GPa with 2 mol% Y_2O_3 to 205 (±5) GPa with 5 mol% Y_2O_3 content. As with relative densities, the Young's moduli of the MWS ZrO_2 materials decrease slightly with Y_2O_3 content, all possessing elastic moduli of ~200–220 (±5–10) GPa. It is clear that the MWS materials, particularly those with lower Y_2O_3 content, are stiffer than their CS counterparts, as a result of their higher density and lower porosity.

Figure 7 shows the effect of Y_2O_3 content on Vicker's hardness which increases linearly, for the CS ZrO_2 materials, from 7 GPa with 2 mol% Y_2O_3 to 11 GPa

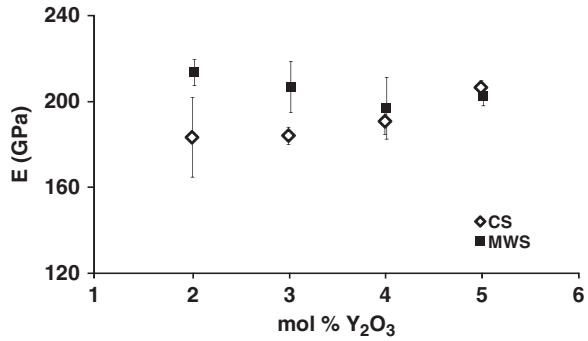

Fig. 6. Effect of Y_2O_3 content on Young's modulus of microwave sintered (MWS) and conventionally sintered (CS) ZrO_2.

with 5 mol% Y_2O_3 content. The hardness values of the MWS ZrO_2 ceramics are all in the range 11.5–12.5 (±0.5–1) GPa, except for ZrO_2 doped with 4 mol% Y_2O_3 which is somewhat lower because of the defects present from sintering. The hardness values for the MWS ZrO_2 ceramics doped with 4 and 5 mol% Y_2O_3 are similar to their CS counterparts.

Figure 8 shows the effects of Y_2O_3 content on BFS of the MWS and CS ZrO_2 ceramics. The BFS decreases from 800 (±80) MPa with 2 mol% Y_2O_3 to 550 (±50) MPa with 3 mol% Y_2O_3 to 420 (±20) MPa with 5 mol% Y_2O_3. The BFS of the CS ZrO_2 with 2 mol% Y_2O_3 is the lowest of all tested at 300 (±200) MPa, whereas the strengths of the CS ZrO_2 with 3–5 mol% Y_2O_3 are all in the range ~430–450 (±30) MPa.

The large differences in strengths between the MWS and CS ZrO_2 with 2 mol% Y_2O_3 is partially due to the differences in density and porosity but may also be influenced by the type of zirconia present, the MWS sample containing mainly *t*-ZrO_2 whereas the CS sample contains mainly *m*-ZrO_2.

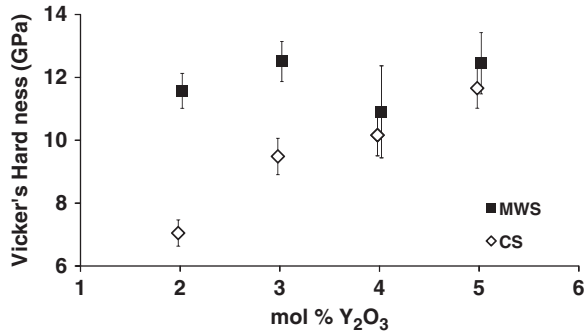

Fig. 7. Effect of Y_2O_3 content on Vicker's hardness of microwave sintered (MWS) and conventionally sintered (CS) ZrO_2.

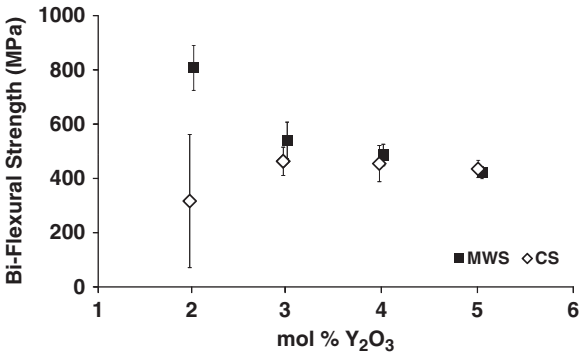

Fig. 8. Effect of Y_2O_3 content on biaxial flexural strength of microwave sintered (MWS) and conventionally Sintered (CS) ZrO_2.

MWS ZrO_2 ceramic doped with 2 mol% Y_2O_3 is the best overall material in terms of density, elastic modulus and, in particular, strength at 800 ($\pm$80) MPa. The increased strength compared with even the MWS ZrO_2 material doped with 3 mol% Y_2O_3 may also be due to the mainly *t*-ZrO_2 microstructure whereas higher Y_2O_3 contents give microstructures containing mixtures of cubic and tetragonal phases. All other compositions have strength values lower than 600 MPa.

SEM and Grain Size

Figure 9 shows SEM of the fracture surfaces of MWS and CS ZrO_2 ceramics doped with 2 mol% Y_2O_3 sintered at 1300°C. The MWS sample (a) indicates that there was greater grain growth and reduction in porosity compared with its CS counterpart (b). As shown in Table II, the average grain size of the MWS ZrO_2 with 2 mol% Y_2O_3 is 353 nm, 75% greater than the CS counterpart. This suggests that there is an enhanced diffusional effect attributed to microwave sintering.

Discussion

The particle size study indicates that ball milling is a suitable technique for producing homogeneously dispersed Y_2O_3–ZrO_2 composite powders at the nanoscale. The larger particle size obtained using particle size analyses compared with the BET details indicate that the ZrO_2 is prone to agglomeration in water. Similar results have been reported with ZrO_2 powders elsewhere.[26] During the course of the microwave heating regime

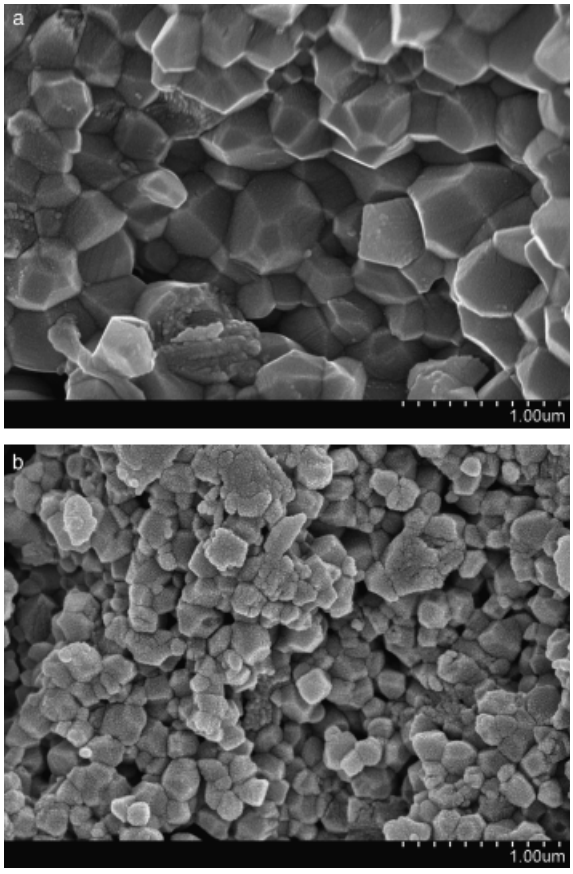

Fig. 9. Scanning electron micrographs of fracture surfaces of ZrO_2 ceramics doped with 2 mol% Y_2O_3 (a) microwave sintered (b) conventionally sintered at 1300°C.

employed, the measured temperature increases in an almost linear fashion up to ~800°C. This initial ramp rate is due to microwave energy being absorbed by the SiC susceptor, which is internally converted to thermal

Table II. Effect of Y_2O_3 Content on Average Grain Size of Microwave and Conventionally Sintered ZrO_2 Samples

	Grain size (nm)			
Sintering	2 mol% Y_2O_3	3 mol% Y_2O_3	4 mol% Y_2O_3	5 mol% Y_2O_3
MWS	353	200	183	180
CS	200	192	206	223

MWS, microwave sintered; CS, conventionally sintered.

Table III. Summary of Properties of MWS and CS Y_2O_3-Doped ZrO_2 Sintered at 1300°C

Sample	Relative density %	Open porosity %	E (GPa)	Hardness (GPa)	Biaxial-flexural strength (MPa)	Grain size (nm)	% Monoclinic phase
MWS							
2 mol% Y_2O_3	97.9	0.5	213 ± 18	11.57 ± 0.55	807 ± 82	353	6
3 mol% Y_2O_3	96.8	1.3	206 ± 11	12.5 ± 0.64	540 ± 67	200	—
4 mol% Y_2O_3	92.7	4.6	194 ± 14	10.4 ± 1.46	486 ± 39	183	—
5 mol% Y_2O_3	95.1	1.4	202 ± 3	12.04 ± .97	421 ± 22	180	—
CS							
2 mol% Y_2O_3	91.4	5.5	183 ± 6	7.04 ± 0.42	316 ± 245	200	86
3 mol% Y_2O_3	93.5	4.2	184 ± 4	9.48 ± 0.56	463 ± 52	192	—
4 mol% Y_2O_3	94	3.5	190 ± 5.9	10.16 ± 0.66	454 ± 66	206	—
5 mol% Y_2O_3	95.1	1.4	206 ± 4.4	11.65 ± 0.63	434 ± 31	223	—

MWS, microwave sintered; CS, conventionally sintered.

energy. The heat is subsequently radiated in a conventional fashion to the surface of the samples. From ~800°C onwards, the SiC becomes transparent to microwave radiation and the ZrO_2 samples begin absorbing the energy directly, which leads to an increase in heating rate.[12,27]

Table III summarizes the properties of all the MWS and CS Y_2O_3-doped ZrO_2 ceramics. The physical and mechanical properties of all the MWS ZrO_2 materials containing up to 4 mol% Y_2O_3 content are improved with respect to their CS counterparts. This is due to the increased densification and reduction in open porosity associated with the microwave heating method. As mentioned in the introduction, the most commonly used structural ZrO_2 ceramic contains 3 mol% Y_2O_3 due to superior flexural strength and fracture toughness.[3] This composition should be the optimum for achieving a single-phase *t*-ZrO_2 with appropriate heat treatments.

In this study, the microstructure of the MWS ZrO_2 ceramic with 2 mol% Y_2O_3 contained mainly *t*-ZrO_2 after MW sintering at 1300°C with flexural strength of 800 (±80) MPa whereas its CS ZrO_2 counterpart contains mainly *m*-ZrO_2 and has lower density and lower strength of 300 MPa with large variability (±200 MPa). The flexural strength of 800 MPa is 50% greater than that for MWS ZrO_2 with 3 mol% Y_2O_3, even though the density is only slightly higher for MWS ZrO_2 with 2 mol% Y_2O_3. SEM imaging of the fracture surfaces and grain size analysis of this MWS material with 2 mol% Y_2O_3 showed much more significant grain growth than its CS counterpart.

Porosity has a significant effect on the physical properties of brittle materials. In the context of mechanical properties, the dependence of Young's modulus, strength and hardness on porosity is generally well described by the following empirical exponential relationship[28]:

$$A = A_0 \exp(-b_A P) \tag{6}$$

where: A_0 is the value of the property at zero porosity, b_A is a measure of the rate of decrease in property, A, with increasing porosity, P.

This equation tends to hold for low to intermediate values, ranging from zero porosity (theoretically fully dense ceramics) to volume fraction porosities of between 0.3 and 0.4.[29] For example, Ren *et al.*[30] demonstrated that the Young's modulus of both Al_2O_3 and hydroxyapatite exhibited this relationship in the porosity region of $0.06 < P < 0.39$ and $0.5 < P < 0.51$ respectively. Díaz *et al.*[22] have also shown a similar dependency for porous silicon nitride. Luo and Stevens[31] also described good agreement between experimental data and empirical relationships for both the hardness and Young's modulus of 3Y–TZP ceramics. In Fig. 10, the Young's modulus is plotted as function of the porosity for all compositions and the line represents the empirical exponential fit. The coefficient of determination ($R^2 = 0.932$), while the zero porosity value (E_0) was 214 GPa (±1.81), and b_E was 0.03 (±0.002). A linear relationship was also examined giving a similar slightly lower coefficient of determination of 0.928 and a similar (E_0) of 214. While the R^2 values are lower than those observed in the case of Al_2O_3 (R^2 of 0.99)[30] and 3Y–TZP (R^2 of 0.985),[31] it

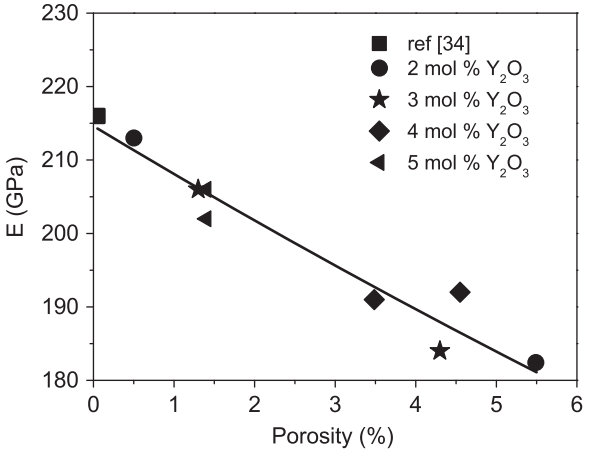

Fig. 10. Young's modulus as a function of porosity for all compositions.

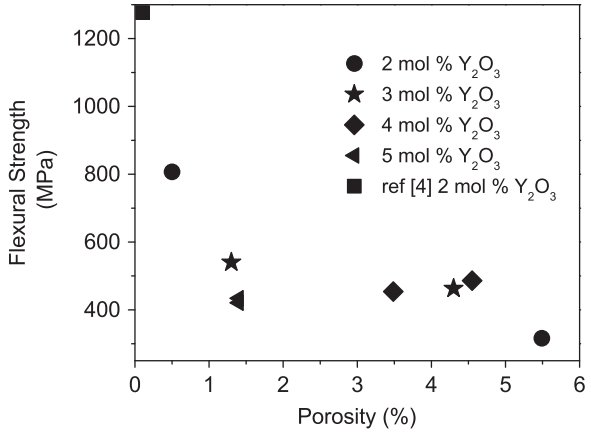

Fig. 11. Biaxial flexural strength as a function of porosity for all compositions.

confirms that it is primarily porosity that affects the Young's modulus of the ZrO_2 not Y_2O_3 content.

The stability of a tetragonal grain inside a tetragonal matrix is controlled by three main factors; the grain size, the matrix constraint, and the amount of stabilizer dopant (in this case Y_2O_3).[32,33] The high porosity of the CS 2 mol% Y_2O_3 may have resulted in reduced matrix constraint and a spontaneous transformation to the monoclinic state. However, in the case of Y–TZP it has been observed that the transformation toughening effect (stress-induced tetragonal to monoclinic phase transformation) is grain-size dependant.[34,35] The larger the grain size the greater the propensity to undergo stress-induced transformation to an equilibrium state and hence the greater the toughening contribution.[2] This correlates with the higher flexural strength of the MWS ZrO_2 with 2 mol% Y_2O_3 compared with 3 mol% Y_2O_3, despite similar densities and retention of the *t*-phase. Figure 11 indicates the effect of porosity on BFS. While the strengths decrease with increases in porosity, the strength–porosity relationship does not follow an exponential trend as with elastic modulus. Thus, the effects of grain size and phase differences due to Y_2O_3 additions also play a major role in relation to strength.

The hardness of a ceramic is typically a function of both porosity and grain size. In terms of porosity it follows the empirical relationship in Eq. (6). However in terms of grain size there is no single trend that applies to every ceramic.[36] Rice *et al.*[37] reviewed the relationship between hardness and grain size for a range of both dense oxide and non-oxide ceramics. It was indicated that there were generally conflicting trends with either hardness exhibiting no grain size dependence, decreasing hardness from single crystals with decreasing grain size or the more generally accepted decrease in hardness with increasing grain size. In the case of ZrO_2, little dependence of H_v on grain size was observed for grain sizes in the range 0.5–50 μm while Al_2O_3 exhibits ~10% reduction in H_v with a 10-fold increase in grain size.[37] Ehre and Chaim[38] also observed differing behavior in nanocrystalline MgO ceramics. Above a grain size of 130 nm, H_v was found to increase with decreasing grain size according to the Hall–Petch relationship. However, below 130 nm any further decrease in grain size leads to a decrease in H_v.

Basu *et al.*[6] observed similar results to those presented here for ZrO_2 produced by hot-pressing similar mixed powders at 1450°C. Increases in flexural strength and fracture toughness were observed as Y_2O_3 content decreased. The addition of Y_2O_3-free *m*-ZrO_2 particles to 3 mol% Y_2O_3 coprecipitated powders resulted in grain growth and increased transformability to *t*-ZrO_2. Yttria from the coprecipitated grains diffuses into the original *m*-ZrO_2 grains resulting in highly transformable tetragonal grains with higher flexural strength and fracture toughness with maximum flexural strength of 1269 MPa for ZrO_2 with 2 mol% Y_2O_3.[6] It was also noted that total Y_2O_3 content must remain above 1.75 mol% to avoid spontaneous transformation to *m*-ZrO_2.

While the maximum flexural strength of 800 MPa achieved in this study for ZrO_2 with 2 mol% Y_2O_3 was

less than the hot-pressed material,[6] it was significantly higher than that for ZrO_2 with 3 mol% Y_2O_3, suggesting that a similar effect occurred in the case of the MWS samples. The continuing reduction in strength as Y_2O_3 content increased is due to the formation of *c*-ZrO_2 at the expense of *t*-ZrO_2. These observations suggest that MWS allows retention of *t*-ZrO_2 phase at a "lower" sintering temperature of 1300°C at which conventional sintering does not stabilize the *t*-ZrO_2 but results in spontaneous reversion to *m*-ZrO_2.

Binner *et al.*[16] observed greater grain growth in ZnO ceramics using a hybrid microwave technique compared with conventional sintering. It was suggested that the "microwave effect" was a simple acceleration of diffusional processes associated with conventional grain growth mechanisms so that it occurs at a lower temperature (by approximately 100°C). In the current study of ZrO_2, microwave sintering resulted in increased density that led to the stabilization of *t*-ZrO_2, together with associated grain growth that did not occur in samples which were CS, despite a similar sintering profile used for both techniques. While the grain growth and densification could be indicative of a higher temperature, the optical pyrometer focused on the surface of the MWS samples did not measure any additional temperature. This suggests that the microwave energy provides an additional driving force during sintering, the so-called "microwave effect" which enhances the diffusional processes within the ceramic. There have been a number of studies reporting such nonthermal microwave effects in ceramic materials and such effects have been reviewed by Bykov *et al.*[27] This effect decreases as the Y_2O_3 content increases to a point where there was no additional enhancement in densification for samples of 5 mol% Y_2O_3 that were MWS. It is envisioned that further study is required to fully densify bodies using higher temperatures and/or longer holding times to establish whether such enhancements can be achieved in near fully dense bodies. Microwave sintering may be beneficial for processing dental grade yttria-doped zirconia ceramics at lower sintering temperatures.

Conclusions

- Attrition milling results in homogeneously mixed nanoscale composite zirconia–yttria powders.
- Microwave radiation can heat yttria-doped zirconia green bodies effectively enough to allow more densification during sintering to occur compared with conventional sintering using the same heating profile particularly in the case of lower Y_2O_3 additions.
- Microwave sintering of Y_2O_3-doped ZrO_2 compacts can yield materials with significantly improved physical and mechanical properties relative to CS counterparts, particularly in the case of 2–3 mol% Y_2O_3 additions.
- Microwave energy can retain *t*-ZrO_2 at "lower" sintering temperatures (1300°C) where, under conventional sintering conditions, *m*-ZrO_2 would be expected to form.
- Microwave sintering leads to enhanced grain growth of ZrO_2 compared with CS counterparts, particularly in the case of material doped with 2 mol% Y_2O_3.
- The improved physical and mechanical properties, along with the different phase assemblages and microstructural evidence, indicate that microwaves provide an extra driving force during sintering which enhances diffusional processes within the Y_2O_3-doped ZrO_2 ceramics, particularly in the case of 2–3 mol% Y_2O_3 additions.

References

1. R. C. Garvie, R. H. J. Hannink, and R. T. Pascoe, "Ceramic Steel," *Nature (London)*, 258 703–704 (1975).
2. P. F. Becher and M. V. Swain, "Grain-Size-Dependent Transformation Behavior in Polycrystalline Tetragonal Zirconia," *J. Am. Ceram. Soc.*, 75 [3] 493–502 (1992).
3. R. H. J. Hannink, P. M. Kelly, and B. C. Muddle, "Transformation Toughening in Zirconia-Containing Ceramics," *J. Am. Ceram. Soc.*, 83 [3] 461–487 (2000).
4. B. Basu, "Toughening of Yttria-Stabilised Tetragonal Zirconia Ceramics," *Int. Mater. Rev.*, 50 [4] 239–256 (2005).
5. S. P. S. Badwal, "Zirconia-Based Solid Electrolytes: Microstructure, Stability and Ionic Conductivity," *Solid State Ionics*, 52 [1–3] 23–32 (1992).
6. B. Basu, J. Vleugels, and O. Van der Biest, "Toughness Tailoring of Yttria-Doped Zirconia Ceramics," *Mater. Sci. Eng. A*, 380 [1–2] 215–221 (2004).
7. J. Wilson and S. M. Kunz, "Microwave Sintering of Partially Stabilized Zirconia," *J. Am. Ceram. Soc.*, 71 [1] 40–41 (1988).
8. S.A Nightingale, H. K. Worner, and D. P. Dunne, "Microstructural Development During the Microwave Sintering of Yttria–Zirconia Ceramics," *J. Am. Ceram. Soc.*, 80 [2] 394–400 (1997).
9. A. Goldstein, N. Travitzky, A. Singurindy, and M. Kravchik, "Direct Microwave Sintering of Yttria-Stabilized Zirconia at 2.45 GHz," *J. Eur. Ceram. Soc.*, 19 [12] 2067–2072 (1999).
10. D. D. Upadhyaya, A. Ghosh, G. K. Dey, R. Prasad, and A. K. Suri, "Microwave Sintering of Zirconia Ceramics," *J. Mater. Sci.*, 36 4707–4710 (2001).
11. D. D. Upadhyaya, A. Ghosh, K. R. Gurumurthy, and R. Prasad, "Microwave Sintering of Cubic Zirconia," *Ceram. Int.*, 27 [4] 415–418 (2001).
12. J. Binner, K. Annapoorani, A. Paul, I. Santacruz, and B. Vaidhyanathan, "Dense Nanostructured Zirconia by Two Stage Conventional/Hybrid Microwave Sintering," *J. Eur. Ceram. Soc.*, 28 [5] 973–977 (2008).
13. J. Wang, *et al.*, "Evidence for the Microwave Effect During Hybrid Sintering," *J. Am. Ceram. Soc.*, 89 [6] 1977–1984 (2006).

14. E. T. Thostenson and T. W. Chou, "Microwave Processing: Fundamentals and Applications," *Composites*, A 30 [9] 1055–1071 (1999).
15. S. Nightingale, "Interfacial Phenomena in Microwave Sintering," *Ionics*, 7 327–331 (2001).
16. J. Binner, *et al.*, "Evidence for the Microwave Effect During the Annealing of Zinc Oxide," *J. Am. Ceram. Soc.*, 90 [9] 2693–2697 (2007).
17. P. D. Ramesh, D. Brandon, and L. Schachter, "Use of Partially Oxidized SiC Particle Bed for Microwave Sintering of Low Loss Ceramics," *Mater. Sci. Eng.*, A 266 [1] 211–220 (1999).
18. H. Toraya, M. Yoshimura, and S. Somiya, "Calibration Curve for Quantitative Analysis of the Monoclinic–Tetragonal ZrO_2 System by X-Ray Diffraction," *J. Am. Ceram. Soc.*, 67 [6] 119–121 (1984).
19. V. Aleksandrov, *et al.*, "Structure of Single Crystals of Stabilized Zirconium Dioxide," *Izv. Akad. Nauk. SSSR Neorg. Mater.*, 12 273–277 (1976).
20. R. P. Ingel and D. Lewis III, "Lattice Parameters and Density for Y_2O_3-Stabilized ZrO_2," *J. Am. Ceram. Soc.*, 69 [4] 325–332 (1986).
21. ASTM Standard E494 10. "Standard Practice for Measuring Ultrasonic Velocity in Materials," Sub-committee E07.06, ASTM International, West Conshohocken, PA, 2010.
22. A. Díaz, S. Hampshire, J.-F. Yang, T. Ohji, and S. Kanzaki, "Comparison of Mechanical Properties of Silicon Nitrides with Controlled Porosities Produced by Different Fabrication Routes," *J. Am. Ceram. Soc.*, 88 [3] 698–706 (2005).
23. ISO Standard ISO6872, *Dentistry—Ceramic Materials*, ISO, Geneva, Switzerland, 2008.
24. P. Jurran, J. Tartaj, and C. Moure, "Sintering Behaviour and Microstructural Evolution of Agglomerated Spherical Particles of High-Purity Barium Titanate," *Ceram. Int.*, 29 [4] 419–425 (2003).
25. R. A. Kimel and J.H. Adair, "Aqueous Synthesis at 200°C of Sub-10 Nanometer yttria Tetragonally Stabilized Zirconia Using a Metal–ligand Approach," *J. Am. Ceram. Soc.*, 88 [5] 1133–1138.
26. M. Hasanuzzaman, A. Rafferty, A. G. Olabi, and T. Prescott, "Sintering and Characterisation of Nanosized Yttia-Stabilised Zirconia," *Int. J. Nanopart.*, 1 [1] 50–65 (2008).
27. Y. V. Bykov, K. I. Rybakov, and V. E. Semenov, "High-Temperature Microwave Processing of Materials," *J. Phys. D: Appl. Phys.*, 34 R55–R75 (2001).
28. R. W. Rice, *Porosity of Ceramics*, Marcel Dekker, New York, 1998.
29. R. W. Rice, *Mechanical Properties of Ceramics and Composites*, Marcel Dekker, New York, 2000.
30. F. Ren, E. D. Case, A. Morrison, M. Tafesse, and M. J. Baumanna, "Resonant Ultrasound Spectroscopy Measurement of Young's Modulus, Shear Modulus and Poisson's Ratio as a Function of Porosity for Alumina and Hydroxyapatite," *Philos. Mag.*, 89 1163–1182 (2009).
31. J. Luo and R. Stevens, "Porosity-Dependence of Elastic Moduli and Hardness of 3Y–TZP Ceramics," *Ceram. Int.*, 25 [3] 281–286 (1999).
32. A. H. Heuer, N. Claussen, W. M. Kriven, and M. Ruhle, "Stability of Tetragonal ZrO_2 Particles in Ceramic Matrices," *J. Am. Ceram. Soc.*, 65 [12] 642–650 (1982).
33. R. C. Garvie and M. V. Swain, "Thermodynamics of the Tetragonal to Monoclinic Phase Transformation in Constrained Zirconia Microcrystals," *J. Mater. Sci.*, 20 [4] 1193–1200 (1985).
34. A. Bravo-Leon, Y. Morikawa, M. Kawahara, and M. J. Mayo, "Fracture Toughness of Nanocrystalline Tetragonal Zirconia with low Yttria Content," *Acta Mater.*, 50 [18] 4555–4562 (2002).
35. F. F. Lange, "Transformation Toughening," *J. Mater. Sci.*, 17 [1] 225–234 (1982).
36. T. P. Hoepfner and E. D. Case, "The Influence of Microstructure on the Hardness of Sintered Hydroxyapatite," *Ceram. Int.*, 29 [6] 699–706 (2003).
37. R. W. Rice, C. C. Wu, and F. Borchelt, "Hardness–Grain-Size Relations in Ceramics," *J. Am. Ceram. Soc.*, 77 [100] 2539–2553 (1994).
38. D. Ehre and R. Chaim, "Abnormal Hall-Petch Behaviour in Nanocrystalline MgO Ceramic," *J. Mater. Sci.*, 43 6139–6143 (2008).